

Sensor clustering technique for practical structural monitoring and maintenance

Ozan Celik^{1a}, Thomas Terrell^{1b}, Mustafa Gul^{2c} and F. Necati Catbas^{*1}

¹Department of Civil Environmental and Construction Engineering, University of Central Florida,
12800 Pegasus Drive, Orlando, FL 32816-2450, USA

²Department of Civil and Environmental Engineering, University of Alberta, 7-257 Donadeo Innovation Centre
for Engineering 9211-116th Street NW Edmonton, Alberta, Canada

(Received February 6, 2018, Revised April 10, 2018, Accepted April 24, 2018)

Abstract. In this study, an investigation of a damage detection methodology for global condition assessment is presented. A particular emphasis is put on the utilization of wireless sensors for more practical, less time consuming, less expensive and safer monitoring and eventually maintenance purposes. Wireless sensors are deployed with a sensor roving technique to maintain a dense sensor field yet requiring fewer sensors. The time series analysis method called ARX models (Auto-Regressive models with eXogeneous input) for different sensor clusters is implemented for the exploration of artificially induced damage and their locations. The performance of the technique is verified by making use of the data sets acquired from a 4-span bridge-type steel structure in a controlled laboratory environment. In that, the free response vibration data of the structure for a specific sensor cluster is measured by both wired and wireless sensors and the acceleration output of each sensor is used as an input to ARX model to estimate the response of the reference channel of that cluster. Using both data types, the ARX based time series analysis method is shown to be effective for damage detection and localization along with the interpretations and conclusions.

Keywords: structural health monitoring; damage detection; wireless sensors; ARX models; time series modeling; sensor roving; practical maintenance

1. Introduction

Development of a sustainable infrastructure will utilize technological advances from various fields and serve as a tremendous benefit to our society. Yet, the condition of our current aging infrastructure and recent natural disasters highlight safety as a current primary concern, calling for efficient inspection and maintenance operations. Structural Health Monitoring (SHM), the research area focusing on condition assessment of different structures, offers a proactive approach to monitoring the state of our infrastructure, aiding in both safety and sustainability. In the past, signal reliability and power supply issues were serious limiting factors for application of wireless

*Corresponding author, Professor, E-mail: catbas@ucf.edu

^a Ph.D., E-mail: ozancelik@knights.ucf.edu

^b M.Sc., E-mail: tomkterrell@yahoo.com

^c Associate Professor, E-mail: mustafa.gul@ualberta.ca

sensors on a full-scale. Research contributions and technological advances in wireless sensor technology have begun to offer wireless sensors as a viable alternative to their wired counterparts (Farinholt *et al.* 2010), although, there are still major questions to be answered. Utilization of wireless sensors encourages further development of damage detection methodologies that implement time series analysis. Time series analysis and other methods can be embedded on the wireless nodes, leading to onboard analysis of data and thus, drastically reducing power supply demands associated with wireless data transfer.

Damage detection refers to a broad research area, and it can be utilized for different purposes, such as validation of the properties of a new structure and long-term monitoring of an existing structure. Damage detection is also a key component of SHM, with a variety of research studies existing which explore various detection methods. A thorough review of civil infrastructure SHM applications and associated damage detection methods can be found in Brownjohn *et al.* (2004). In this study, the types of damage measured are limited specifically to those most commonly experienced by bridges: boundary condition changes of the structure and local stiffness loss. Damage of these types is typically the result of structural or material altering processes, for example: corrosion or scour. However, the type of damage capable of being detected, using the methodology presented in this study, is not limited to only these two types. Any damage resulting from a structural or material change that affects the dynamic properties of a structure during the monitoring period, in theory, can be identified using the presented methodology. In addition, it is also important to have a gage for the success of a damage detection methodology. An effectiveness of a given methodology is defined at four levels, which are: (1) detection of the damage, (2) localization of the damage, (3) quantification of damage, and (4) decision making.

Time or frequency based conventional parametric damage detection methods are generally dependent on the estimation of modal parameters. The obtained modal parameters may either directly be used or their derivatives may be used as damage sensitive metrics. Some of the common modal parameter-based features may be summarized as the natural frequencies, mode shapes and their derivatives, modal flexibility matrix, modal curvature and others (Dessi and Camerlengo 2015, Gillich and Prasiach 2014, Gul 2009). It has been shown that these metrics are hard to compare as they outperform each other based on environmental or structural conditions and may not be as sensitive as they were thought especially when localized damages are of concern. Review of the literature shows that use of Auto-Regressive with eXogeneous input (ARX) models for SHM could be an effective alternative since their implementation for an automated SHM system is relatively more feasible compared to other damage detection methodologies such as parametric (physics-based) or model updating (Gul and Catbas 2009). This analysis approach mainly fits time series models to the vibration data and then aims to detect the damage by extracting features such as curve fit coefficients or error terms. In other words, some of these methodologies directly compare the time series models whereas some of them use the residual errors when the new data is used with the previously created model. These methodologies usually make use of Auto-Regressive (AR) and ARX models to detect the damage in a statistical manner (Gul 2009).

However, the use of time series models, in general, for damage detection is not a new concept. Sohn and Farrar (2001) introduced a novel approach to damage detection, which modeled dynamic signals recorded on two different mechanical systems under various damage conditions using Autoregressive (AR) time series models. From statistical examination of changes in the AR model coefficients, they were able to identify data coming from a damaged system. The results of this early study provided inspiration for similar research. For example, in the study by Omenzetter and

Brownjohn (2006), Auto-Regressive Integrated Moving Average (ARIMA) models were used to analyze static strain data from a bridge in service and during its construction. The results of this study again demonstrated the capability of using time series models as a damage detection method; although, it also revealed limitations of the methodology in detecting the nature, severity and location of damage.

Another study used Auto-Regressive Moving Average (ARMA) models and a statistical pattern classifier, which was based on analysis of the structure's response in the time domain. The statistical classifier algorithms were trained using the coefficients from the ARMA model. The approach was demonstrated on three different experimental structures, and in all investigations, was found to be capable of identifying structural change and separating different damage cases from one another.

Time series based damage detection methodologies have also been utilized in conjunction with wireless sensor technology. Some of the most relevant wireless technology research is summarized in the following studies. A recent study by Sazonov *et al.* (2010), addressed the issue of ensuring synchronous data acquisition across wireless nodes in large, spatially distributed networks. Time synchronization of sensor-acquired vibration responses is essential for application of mode shape-based damage detection; yet, synchronization is a challenge as network size increases. In the study, a detailed description of a novel wireless sensor network architecture is provided, which was shown, through field application on a bridge in New York, to be capable of reconstructing the mode shapes of the structure (Sazonov, *et al.* 2010). This study is an example of the type of research that is improving the practical implementation of wireless sensor technology in SHM systems.

The study conducted by Tanner (2003), provides a perspective of one of the commercially available wireless sensor systems and associated capabilities at that time. In this study a wireless sensor system referred to as "Motes", developed at University of California Berkeley, was employed on a limited scale laboratory structure. Despite the researchers demonstrating an AR-ARX algorithms' (Sohn *et al.* 2000) success using a traditional wired DAQ system, implementation of the same method was unsuccessful in the off-the shelf wireless system. Several reasons for this "failure" are provided and include: limited sensor resolution range, inability of system to simultaneously sample multiple channels, and limited flash memory size. It, however, was stated that most of these issues could be easily remedied by selecting sensors and an analog-to-digital converter that were better suited to the application (Tanner 2003). A comprehensive review of wireless SHM for civil structures references an academic prototype in 2003 that may in fact have been capable of handling complex algorithms (Lynch 2007). The question remains, though, to whether these proper capabilities were available in a commercially available wireless sensor.

One of the earliest examples of a successful full-scale field application of a wireless sensor network is provided by Lynch *et al.* (2004). In this study, a wireless sensor network employed on an isolated highway bridge, tested under impact loading from an impact hammer, is described. The sensors were equipped to execute an on-board FFT analysis of the forced vibration response time-history data. The researchers were successful in identifying the primary modal frequencies, as shown through validation of both the time history data and frequency domain signals with a traditional parallel installed wired system (Lynch *et al.* 2004).

Recent advances in the application of time series analysis damage detection methodologies are described by Zheng and Mita (2009). Their research utilizes the distance measures of AR models as damage indicators in an experimental study. The Itakura Distance and Cepstral Distance, both

initially developed to measure the similarities between voice segments, were applied to vibration data collected from a 5-story steel structure subjected to ambient vibration from a shaker table. The results from the study suggested the need for the use of a pre-whitening filter. Nonetheless, from this method, it was concluded that damage in the structure could be detected and localized with sufficient confidence (Zheng and Mita 2009).

One of the most intriguing studies utilizing wireless sensors for SHM is by Pakzad and Fenves (2009). In this study, the researchers deployed a dense network of 64 wireless accelerometers for a period of 3 months on the Golden Gate Bridge. Including testing and debugging, there were a total of 174 data collection runs of the network. The data was analyzed using both the peak picking method and an ARMA model. The ARMA model was used for extraction of the vibration modes of the main span from ambient vibration data. The high spatial density of the sensor network allowed for accurate identification of the first three modes in each direction.

Time series analysis methods using AR, ARX and ARMA models are examples of damage detection methodology options, and they have been employed by various researchers (Sohn and Farrar 2001, Lu and Gao 2005, Omenzetter and Brownjohn 2006). These offer the distinct advantage of requiring only data from the undamaged structure during the training phase. In a prior research study, the authors proposed a time series methodology implementing ARX models (Gul and Catbas 2009) and then improved the same algorithm (Gul and Catbas 2011) with an approach that gives very promising results for detecting, locating and estimating the extent of the damage. As the continuation of the previous studies, the proposed methodology aims to expand the algorithm to be used with wireless sensors and on a more complex structure containing structural decking, where the system's degrees of freedom are not as clearly defined. Furthermore, a roving technique in which wireless sensors are moved to adjacent locations in the presence of limited number of sensors is utilized allowing possible damages along large-scale structures to be estimated with a few number of sensors. The current study also compares the performance of damage estimation results for both wired and wireless acceleration sensor measurements.

2. Time series modeling

Time series modeling is the statistical modeling of a sequence of data points that are measured at successive times spaced at uniform time intervals. Time series modeling makes it possible to model a system that cannot be easily modeled based on physical insights. A variety of standard models have been developed, which by experience are known to be able to handle a wide range of different system dynamics. If it is assumed that the noise and input are subjected to the same dynamics, the relationship between the system's input, output, and error terms can be represented by a linear time series model using the difference equation shown in Eq. (1) (Ljung 1999).

$$\begin{aligned} y(t) + a_1 y(t-1) + \dots + a_{n_a} y(t-n_a) \\ = b_1 u(t-1) + \dots + b_{n_b} u(t-n_b) + e(t) + c_1 e(t-1) + \dots + c_{n_c} e(t-n_c) \end{aligned} \quad (1)$$

where, $y(t)$ is the model output, $u(t)$ is the noise-free input to the model, and $e(t)$ is the error term. The coefficients, a_i , b_i , and c_i are the unknown model parameters, and the model orders are given by n_a , n_b , and n_c . It is assumed that the components comprising the error term are independent and identically distributed (i.i.d.). A reduced form of this equation is shown in Eq. (2).

$$A(q)y(t) = B(q)u(t) + C(q)e(t) \quad (2)$$

where, $A(q)$, $B(q)$, and $C(q)$ are polynomials in the shift, or delay, operator q^{-1} as shown in Eq. (3) below.

$$\begin{aligned} A(q) &= 1 + a_1q^{-1} + a_2q^{-2} + \dots + a_{n_a}q^{-n_a} \\ B(q) &= 1 + b_1q^{-1} + b_2q^{-2} + \dots + b_{n_b}q^{-n_b} \\ C(q) &= 1 + c_1q^{-1} + c_2q^{-2} + \dots + c_{n_c}q^{-n_c} \end{aligned} \quad (3)$$

The model shown in Eq. (2) is referred to as an ARMAX model. $A(q)y(t)$ represents an Auto Regression, $C(q)e(t)$ represents a Moving average of noise, and $B(q)u(t)$ represents an external input. By adjusting the model orders, different time series models are defined. The ARX model, which is used in this study, is obtained by setting n_c equal to zero. In other words, the disturbance dynamics are not modeled. The ARX model structure is shown in Eq. (4).

$$A(q)y(t) = B(q)u(t) + e(t) \quad (4)$$

where, again, $y(t)$ is the model output, $u(t)$ is the noise-free input to the model, and $e(t)$ is the error term.

Instead of an ARMAX model, the ARX model was the type of time series model selected for this study, since modeling of the disturbance dynamics did not affect the end results significantly (Gul 2009). ARX model estimation is one of the most efficient of the polynomial estimation methods due to the fact that it is the result of solving linear regression equations in analytic form (Instruments 2009), thus, suggesting it as a preferred selection in SHM applications. For this study, the model order of the output, n_a , was set to one, since in the utilized methodology it was only necessary to describe the output at individual time steps. The remaining model order, n_b , pertains to the number of previous input values used. This model order (generally shown with p) determines the number of past values used to estimate the value at t (Box *et al.* 1994). The next section describes time series modeling as it relates to structural dynamics.

2.1 Time series modeling for structural dynamics

It is seen from Eq. (4) that a time-series ARX model describing a physical structure can be developed if both the inputs and outputs of the system for a time series are defined. While the structure's outputs can be defined easily enough using available sensing technology, defining the structure's inputs becomes an issue of practicality for SHM of civil infrastructure. Therefore, developing methodologies to extract damage features from output-only data is very important for such applications. A time series based methodology to detect and locate damage using output-only data was proposed by Gul and Catbas (2011). The core premise of the methodology, presented in that study and used in this study, is that output of a degree of freedom (DOF) for a linear dynamic system is related to the outputs of the neighboring DOFs. In other words, the neighboring DOF outputs can be used as inputs in the development of a time series model. In terms of use with the ARX model, the input term $u(t)$ in Eq. (4) can be expressed by a series of our system's outputs. This concept is explained by examining the equation of motion for an N DOF linear dynamic system, shown in Eq. (5) and expressed in expanded matrix form in Eq. (6) (time, t is omitted).

$$[M]\ddot{x}(t) + [C]\dot{x}(t) + [K]x(t) = f(t) \quad (5)$$

$$\begin{bmatrix} m_{11} & \cdots & m_{1N} \\ \vdots & \ddots & \vdots \\ m_{N1} & \cdots & m_{NN} \end{bmatrix} \begin{Bmatrix} \ddot{x}_1 \\ \vdots \\ \ddot{x}_N \end{Bmatrix} + \begin{bmatrix} c_{11} & \cdots & c_{1N} \\ \vdots & \ddots & \vdots \\ c_{N1} & \cdots & c_{NN} \end{bmatrix} \begin{Bmatrix} \dot{x}_1 \\ \vdots \\ \dot{x}_N \end{Bmatrix} + \begin{bmatrix} k_{11} & \cdots & k_{1N} \\ \vdots & \ddots & \vdots \\ k_{N1} & \cdots & k_{NN} \end{bmatrix} \begin{Bmatrix} x_1 \\ \vdots \\ x_N \end{Bmatrix} = \begin{Bmatrix} f_1 \\ \vdots \\ f_N \end{Bmatrix} \quad (6)$$

where, $[M]$ is the mass matrix, $[C]$ is the damping matrix, and $[K]$ is the stiffness matrix. The vectors $\ddot{x}(t)$, $\dot{x}(t)$, $x(t)$, and $f(t)$ are acceleration, velocity, displacement, and the external forcing functions respectively. If the first row of Eq. (6) is expressed separately, the force term eliminated for free response case, and then rearranged, as in Eqs. (7) and (8), it is shown that the free-response acceleration output of the 1st DOF is expressed by the excitation force on the 1st DOF, physical parameters of the structure, and the outputs of the other DOFs.

$$(m_{11}\ddot{x}_1 \cdots m_{1N}\ddot{x}_N) + (c_{11}\dot{x}_1 \cdots c_{1N}\dot{x}_N) + (k_{11}x_1 \cdots k_{1N}x_N) = f_1 \quad (7)$$

$$\ddot{x}_1 = -\frac{(m_{12}\ddot{x}_2 + \cdots + m_{1N}\ddot{x}_N) + (c_{11}\dot{x}_1 + \cdots + c_{1N}\dot{x}_N) + (k_{11}x_1 + \cdots + k_{1N}x_N)}{m_{11}} \quad (8)$$

Therefore, each row of Eq. (6) can be thought of as a sensor cluster, composed of a reference DOF and its surrounding DOFs. Based on these concepts, if different ARX models are created for different clusters of sensors, then damage features can be selected for each of these models to detect damage. In the ARX model expressed in Eq. (5), the $y(t)$ term is the free-response acceleration of the reference channel of a sensor cluster, $u(t)$ is the free-response acceleration responses of all the DOFs in the same cluster, and $e(t)$ is the error term. To be clear, the development of Eq. (8) is only valid if we are considering a free response of the structure case, where the forcing term of Eq. (6) can be eliminated. An infinite number of force inputs could be applied to the structure to generate a free-response; however, application of an impulse force of very short duration is the most preferred type of input, in general. A primary reason for this preference is that a very short duration impulse force in a given range of magnitudes is easy to consistently apply. In addition, a properly applied impulse force on the structure will excite many of the structural modes, thus ensuring that the free decay time response data is descriptive of the entire structural system.

2.2 Damage Feature (DF)

As discussed earlier, numerous approaches exist for extracting damage features from SHM data using a time series analysis. The damage feature(s) itself, however, also varies. In Gul and Catbas (2011), two different types of damage features (DFs) were extracted from the ARX models. The first approach was based on a direct comparison of the “B” term coefficients of the ARX model. While this method was demonstrated to be successful at giving exact information about the existence, location, and severity of the damage for simple models, this approach was not effective for complex models or with addition of data noise. The second approach used the difference in the ARX model fit ratios, Eq. (9), as the DF (Gul and Catbas 2011).

$$\text{Damage Feature (DF)} = \frac{FR_{\text{Healthy}} - FR_{\text{Damaged}}}{FR_{\text{Healthy}}} \times 100 \quad (9)$$

where the fit ratio is expressed by Eq. (10).

$$\text{Fit Ratio (FR)} = \left(1 - \frac{\| \{y\} - \{\hat{y}\} \|}{\| \{y\} - \{\bar{y}\} \|} \right) \times 100 \quad (10)$$

$\{y\}$ is the measured output, $\{\hat{y}\}$ is the predicted output, $\{\bar{y}\}$ is the mean of $\{y\}$ and $\| \{y\} - \{\hat{y}\} \|$ is the norm of $\{y\} - \{\hat{y}\}$.

This method proved to be much more effective for extracting information about the existence and location of the damage for more complex models. It also gave information about the relative severity of the damage; although, direct damage quantification was not achieved. For this reason, the approach using the fit ratio will be used for identifying damage from the laboratory data. Fig. 1 shows a flowchart of how the DF is obtained in this study at a single sensor location for a single data trial. In this way, DF's can be found for all sensor locations, providing a display of which locations have potential damage.

First, a sensor cluster composed of a reference channel and adjacent channels must be defined. The sensor clusters defined must be the same for all conditions. The reference channel represents the location for which a DF will be developed. In this study, a reference channel represents a specific accelerometer location. Next, the total size of the sensor cluster is defined by selecting the adjacent channels, which in this study correspond to neighboring accelerometers. This selection may vary depending on the structure type, but for the purposes of this study, it was found that selecting only adjacent channels that were very close to the reference channel proved to be most effective. Acceleration data is collected from the structure under healthy/baseline conditions. The ARX Baseline model parameters are defined and the adjacent channel acceleration data is then used to create a baseline ARX model. This model is then used to predict the acceleration for the reference channel. A fit ratio is determined by comparing this predicted acceleration to the actual reference channel acceleration. This is known as the healthy fit ratio, FR_{Healthy} . Since the baseline ARX model was developed using the healthy condition acceleration data, as long as the structural conditions remain the same, then the predicted acceleration for the reference channel should very closely fit the actual reference channel acceleration, resulting in a high fit ratio.

Acceleration data from the same defined sensor clusters is continuously collected, and the adjacent channel acceleration data is input into the baseline ARX model. Again, the model-predicted reference channel acceleration is compared to the actual reference channel acceleration and a fit ratio is found. Each new fit ratio is compared to the healthy fit ratio and a DF is generated. For a healthy structure, all new predicted reference channel acceleration data should remain to be in close fit with the actual reference channel acceleration, resulting in a high fit ratio and thus, a low DF value. However, if the properties of the structure change, then it is anticipated that the predicted reference channel acceleration will no longer fit closely with the actual reference channel acceleration, resulting in a lower fit ratio and thus, a high DF value. In addition to the DF's alone as indicators of damage, another method utilizing the DF's was used in this study to better visually display the presence and severity of damage at a particular sensor location. The plot that is generated is called the Averaged DF Distance plot. For better ease of understanding, this method, along with the associated equation, will be discussed in more detail in the following sections.

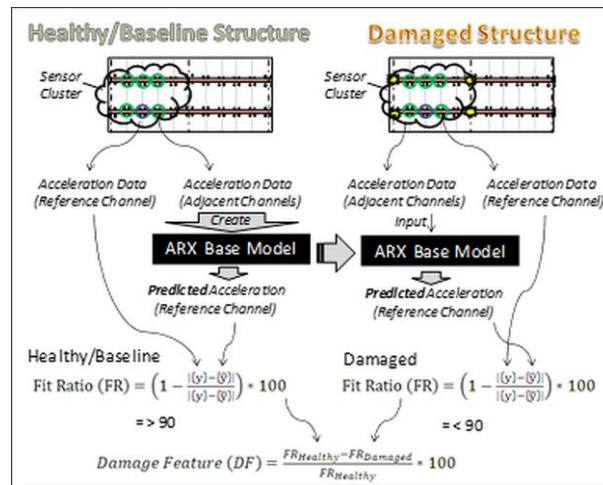


Fig. 1 Flowchart of damage feature determination

3. Laboratory studies

3.1 4-Span bridge-type structure

The laboratory setup used in this study was a 4-span bridge-type structure, shown in Fig. 2. Its responses are representative of typical values for medium-span bridges (Zaurin 2009). The structure serves as a platform for testing and evaluating new sensing technologies, data collection systems, and damage detection algorithms, in a controlled environment, prior to full-scale implementation. It has two 120 cm approach end spans (Fig. 2 (left) (Shaded in Blue)) and two 304.8 cm main inner spans. Only the two inner spans were instrumented with sensors and analyzed for damage. Two HSS 25x25x3 girders, separated 60.96 cm from each other, support a 3.18 mm thick, 120 cm wide steel deck. The steel deck is connected to the girders using sets of four ¼ inch bolts and plates. Through this configuration the girders are only connected to one another by means of the deck. The supports can easily be changed to roller, pin, or fixed boundary conditions, and the girder deck connection can be adjusted at different locations by removing bolts to modify the stiffness of the structure (Fig. 2(right)).

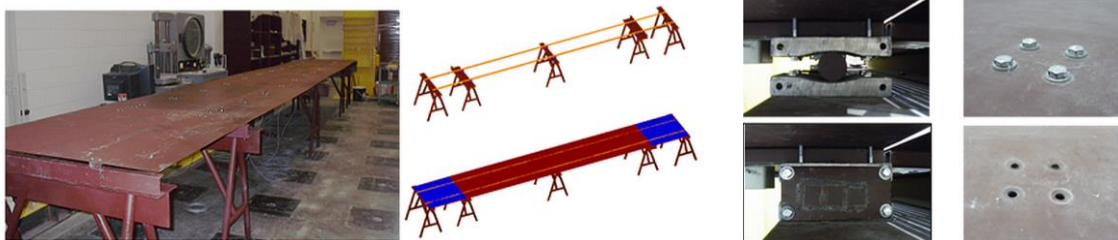


Fig. 2 4-Span Structure in lab and schematic of structure (left); interchangeable supports and bolts (right)

Table 1 Inputs and outputs of the ARX models

| Sensor Cluster | Output of the ARX Model (Reference Channel) | Inputs of the ARX Model (Adjacent Channels) |
|----------------|--|--|
| 1 | N1 | N1, N2, N9, N10 |
| 2 | N2 | N1, N2, N3, N9, N10, N11 |
| 3 | N3 | N2, N3, N4, N10, N11, N12 |
| 4 | N4 | N3, N4, N5, N11, N12, N13 |
| 5 | N5 | N4, N5, N6, N12, N13, N14 |
| 6 | N6 | N5, N6, N7, N13, N14, N15 |
| 7 | N7 | N6, N7, N8, N14, N15, N16 |
| 8 | N8 | N7, N8, N15, N16 |
| 9 | N9 | N1, N2, N9, N10 |
| 10 | N10 | N1, N2, N3, N9, N10, N11 |
| 11 | N11 | N2, N3, N4, N10, N11, N12 |
| 12 | N12 | N3, N4, N5, N11, N12, N13 |
| 13 | N13 | N4, N5, N6, N12, N13, N14 |
| 14 | N14 | N5, N6, N7, N13, N14, N15 |
| 15 | N15 | N6, N7, N8, N14, N15, N16 |
| 16 | N16 | N7, N8, N15, N16 |

3.2 Wired/Wireless sensor and configurations

For the wired accelerometer configuration, a total of sixteen PCB accelerometers, model 603C01, were installed along the bottom of the two girders. These sensors provide a measurement range of ± 50 g and a broadband resolution of 350 μ g and remained attached to the structure at these locations during the entirety of the testing. A total of 16 different sensor clusters were created, one for each reference channel which are summarized in Table 1. The node numbers corresponding to each cluster can be observed in Fig. 4.

The wireless sensors used in the laboratory experiment were the Imote2 accelerometers, which consist of 4 main components: an Imote2 main board that provides the radio and processor, an ISM400 (formerly SHM-A) sensor board, a battery board, and an Antenova Mica 2.4 GHz SMD external antenna. Each Imote2 sensor was attached securely to a circular aluminum base plate, which was then affixed to the four-bolt deck-grid connection using hot glue. Fig. 3 shows installed Imote2 sensors. This sensor provides user selectable sample rates of 25, 50, 100, and 280 Hz and anti-aliasing filters.

Wireless accelerometers collected acceleration data from the same 16 sensor locations shown in Fig. 4, however, since only eight wireless accelerometers were available during the experiments, data collection was performed using a roving technique. This roving technique consisted of collecting data from a set of seven Imote2 sensors in six separate sensor configurations, each requiring its own testing. While in comparison to the wired accelerometers this did increase the total testing time quite significantly, however, it also provided the same sensing mesh density, while only using half the sensor quantity. It was felt that such a roving technique would prove quite useful in real-life SHM applications, where sensor mesh density is a constraint and sensor quantities are an issue.

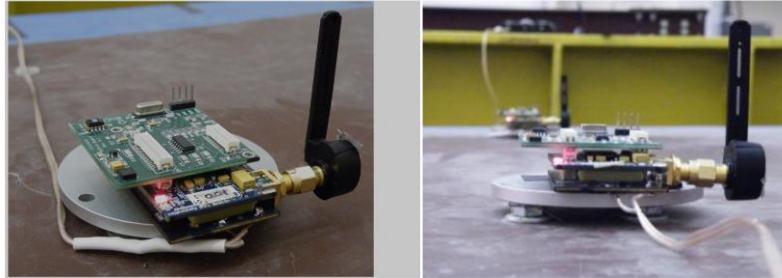


Fig. 3 Installed Imote2 wireless accelerometers

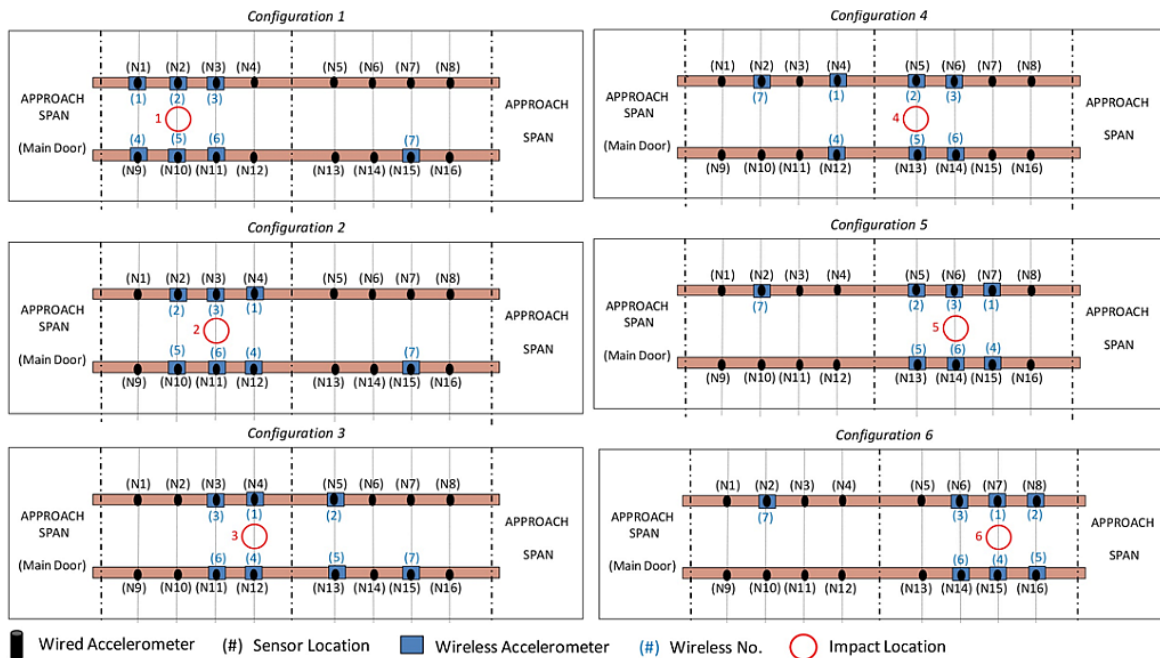


Fig. 4 Sensor configurations and impact locations

The six sensor configurations seen in Fig. 4 allow for the exact same sensor cluster definitions as in the wired accelerometers. The key difference is that the data used for each baseline ARX model development was collected from different testing trials. The 16 defined sensor clusters, one for each reference channel, are summarized in Table 2 in terms of Wireless sensor number and configuration (Convention: Configuration – Wireless Sensor Number).

Fig. 4 shows the six configurations for the wireless accelerometers with reference to the attached wired accelerometers. Note that each configuration contains a seventh sensor that serves as a referencing node, aiding in providing data from the entire structure. Information from this referencing node, although not used in this study, can be later used to splice data from the individual trials together.

Table 2 Inputs and outputs of the ARX models

| Sensor Cluster | Reference Channel (Config. – Sensor No.) | Adjacent Channels (Config. – Sensor No.) |
|----------------|---|---|
| 1 | 1-1 | 1-1, 1-2, 1-4, 1-5 |
| 2 | 1-2 | 1-1, 1-2, 1-3, 1-4, 1-5, 1-6 |
| 3 | 2-3 | 2-1, 2-2, 2-3, 2-4, 2-5, 2-6 |
| 4 | 3-1 | 3-1, 3-2, 3-3, 3-4, 3-5, 3-6 |
| 5 | 4-2 | 4-1, 4-2, 4-3, 4-4, 4-5, 4-6 |
| 6 | 5-3 | 5-1, 5-2, 5-3, 5-4, 5-5, 5-6 |
| 7 | 6-1 | 3-1, 3-2, 3-3, 3-4, 3-5, 3-6 |
| 8 | 6-2 | 6-1, 6-2, 6-4, 6-5 |
| 9 | 1-4 | 1-1, 1-2, 1-4, 1-5 |
| 10 | 1-5 | 1-1, 1-2, 1-3, 1-4, 1-5, 1-6 |
| 11 | 2-6 | 2-1, 2-2, 2-3, 2-4, 2-5, 2-6 |
| 12 | 3-4 | 3-1, 3-2, 3-3, 3-4, 3-5, 3-6 |
| 13 | 4-5 | 4-1, 4-2, 4-3, 4-4, 4-5, 4-6 |
| 14 | 5-6 | 5-1, 5-2, 5-3, 5-4, 5-5, 5-6 |
| 15 | 6-4 | 3-1, 3-2, 3-3, 3-4, 3-5, 3-6 |
| 16 | 6-5 | 6-1, 6-2, 6-4, 6-5 |

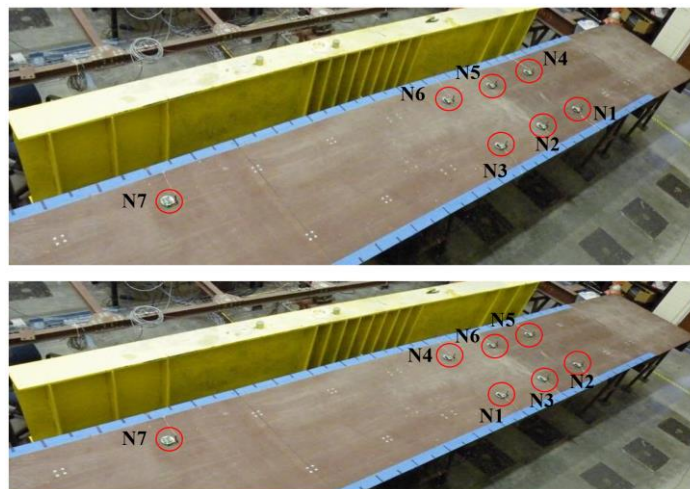


Fig. 5 Wireless sensor configurations 1 and 2 on 4-span structure; Configuration 1 (Top) and configuration 2 (Bottom)

A total of three impact data sets containing 5 impacts each were collected for all 6 sensor configurations under each damage scenario. The PCB Model 086D20 short-sledge impact hammer was used. The impact was applied to the decking of the 4-span structure in the middle area between the two girders, rather than above each girder. The impact locations for each sensor configuration are shown by the red circles in Fig. 4. Pictures of the first two configurations are shown in Fig. 5.

The two sensor types require separate and very different Data Acquisition Systems for proper collection of acceleration data. For the wired configuration, the 16 PCB accelerometers were connected individually to an acquisition system from VXI and Agilent Technologies and the data was sampled at 320 Hz. The sensor network, interface/debug board, USB cable and PC are the only hardware comprising a complete wireless DAQ. The software necessary for an operable wireless network, however, is more complex than its wired counterpart. In this study, a sampling rate of 280 Hz was used for all data collection using the Imote2 wireless accelerometers.

Signal quality was a major concern with using the wireless accelerometers for this time series analysis-based damage detection method. To validate the signal as adequate for use with this method, the wireless signal from the 4-span structure was compared to a corresponding wired accelerometer signal in both time and frequency domains. During testing of the 4-span structure, only acceleration data from the z-axis was collected by the wireless accelerometers, since the wired accelerometers were uniaxial. It should be noted that a noticeable difference can be expected between the wired and wireless data, as a result of the difference between the installation locations of each sensor. The wired accelerometers were installed on the underside of the girders, while the wireless accelerometers were installed on the topside of the girder, but on top of the bolted connection (Fig. 6). Fig. 7 shows a single impact test at node N12. Results of the verification study show that there is sufficient correlation between the wired and wireless signals.

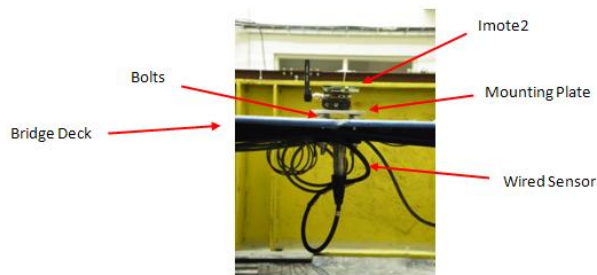


Fig. 6 Wired Vs Wireless accelerometer installation locations

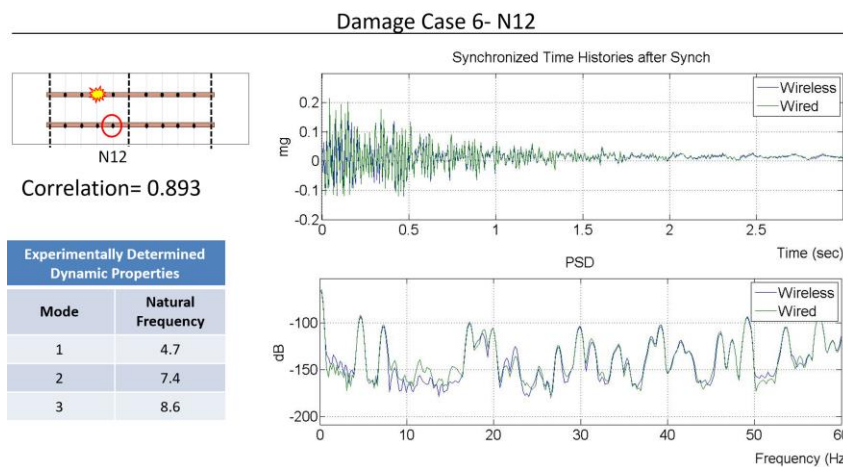


Fig. 7 Time history and Power Spectrum Density (PSD) comparison for node N12

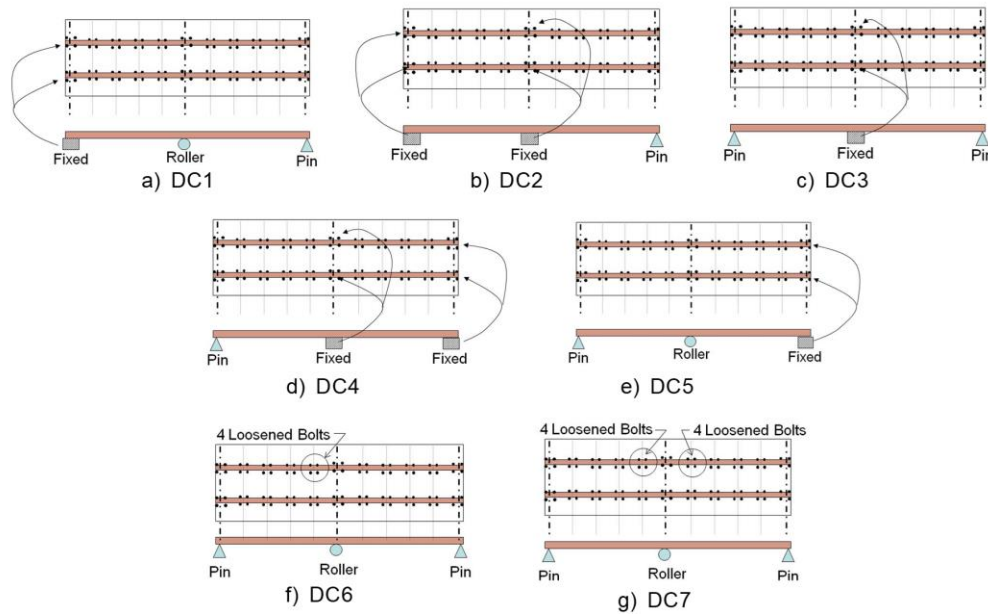


Fig. 8 The seven applied damage scenarios (DC1-DC7)

3.3 Experimental method

During testing, acceleration data was collected simultaneously from both the wired and wireless accelerometers using two separate DAQ systems. While it is possible to determine the input into the system for each impact trial, through measurement of the forces at the hammer tip, in this study, data was not recorded from the hammer tip and the input was left as an unknown. The reason for this is that, as previously stated, the input of the ARX model is simply the acceleration output of the adjacent channel sensors.

Seven separate damage cases were implemented on the laboratory setup and are shown in Fig. 8. Based on feedback from Department of Transportation (DOT) engineers, these damage cases represent some of the most common damages affecting bridge performance. Cases 1- 5 involve changes in the boundary conditions to fixed connections and can therefore be considered global damage. Damage of this type is representative of when roller or pin supports of a bridge experience corrosion or are blocked by debris. Case 1 (Fig. 8(a)) modified the boundary conditions from a pin connection at the left support to a fixed connection. Case 2 (Fig. 8(b)), expanded the damage from Case 1 to also modify the boundary conditions at the middle support from a roller to a fixed connection. Case 3 (Fig. 8(c)) applied a fixed connection to only the middle support, and Cases 4 and 5 (Figs. 8(d) and 8(e)) were symmetrical versions of DC1 and DC2. Cases 6 and 7 simulate localized damage with loss of connectivity between the girder and deck. In Case 6 (Fig. 8(f)), 4 bolts, corresponding to a single grid-deck connection point, were removed. In Case 7 (Fig. 8(g)), a total of eight (8) bolts were removed (4 each) at two girder-deck connections.

4. Results and Interpretations

4.1 Model order selection and threshold determination

Complete analysis of the data can be divided into 4 main steps: (1) Collection, archival and pre-processing of raw data, (2) ARX Baseline model development and generation of DF's, (3) Threshold determination, and (4) Damage identification plots creation.

For the wired sensor data, the model order, p , of the Baseline ARX was determined through an iterative process. Model orders of $p=20, 30, 40, 50$, and 70 were all investigated. However, a model order of $p=50$ was selected due to optimization between high fit ratios and processing time. This model order was used to develop all wired sensor Baseline ARX models. The results shown correspond to the first data set, which consists of 5 impact trials. The Baseline ARX model parameters for the wireless sensors were also determined through an iterative process. Model orders of $p=20, 30, 40, 50, 70, 100$ and 120 were all investigated. However, a model order of $p=70$ was selected due to optimization between high fit ratios and processing time. This model order was used to develop all wireless sensor Baseline ARX models. It should be noted that in order to eliminate problems with the ARX model generation, a 3% white noise was added to the signal. While the addition of noise may appear counter-intuitive, this procedure of adding noise was found to be helpful in previous studies that had problems generating ARX models. Likewise, this addition of noise is accounted for by development of the threshold level. The results shown correspond to a data set consisting of 5 impact trials. Very similar results were generated when using 15 impact trials. Using the larger data set helped to average-out minor variations amongst the 5 individual impact trials. However, it was decided to generate the results using only 5 impact trials in order to demonstrate application of the method.

Prior to damage identification with noisy data, a threshold for the DF must be established to distinguish changes in the DF due to damage from changes as a result of noise in the data. To determine the threshold level, the DFs of at least one undamaged, baseline, data set are found with respect to another undamaged, baseline, data set and plotted. The DFs resulting from the one baseline compared to another baseline represent the amount of noise in the system. A single threshold value is then selected based on this DF trend plot. This value then serves as a reference for any future DF's, with a value above the threshold indicating the potential for damage. The DFs and determined threshold value for wired and wireless sensor measurements for DC0 are shown in Fig. 9.

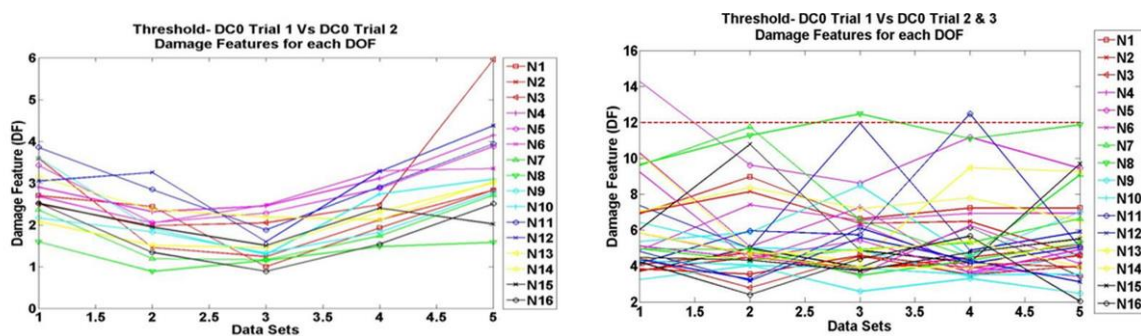


Fig. 9 Threshold level for wired (left) and wireless (right) clusters for the baseline case

4.2 Averaged damage feature distance plots

While the DF trend plot can be used for detecting damage at a particular sensor location, the process is somewhat time consuming and does not visually present the data in an informative way. Therefore, another method, that visually displays the presence and severity of damage at a particular sensor location in a bar chart format, was used. This Averaged DF Distance Plot condenses the series of DF's for a sensor location in the DF trend plot into a single representative value. Under a certain damage case, for a specific sensor cluster and for a certain channel/location (dof), data sets (several trials) for the time interval $t_0 < t < t_1$ are collected and DFs for these different trials are calculated. If the calculated DFs are under the pre-determined threshold value-which was calculated for the baseline case-, then they are marked as inliers and their mean value is calculated accordingly (Fig. 10). Similarly, the mean of the outlier DF values for another data set corresponding to the interval $t_1 < t < t_2$ is also computed. The difference between the mean of the two sets is the Averaged DF Distance. Once this procedure is completed for the desired sensor location/dof, it is repeated until averaged DF distances are determined for all the remaining locations corresponding to that specific damage case. At the end, the obtained distances are represented with bar charts over the entire structure indicating the severity by looking at their magnitude and the location by looking at where they are concentrated.

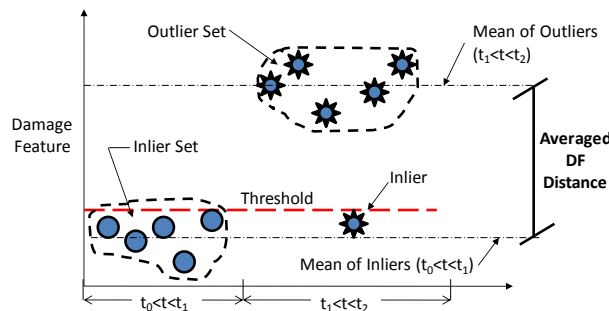


Fig. 10 Distance between two damage feature sets

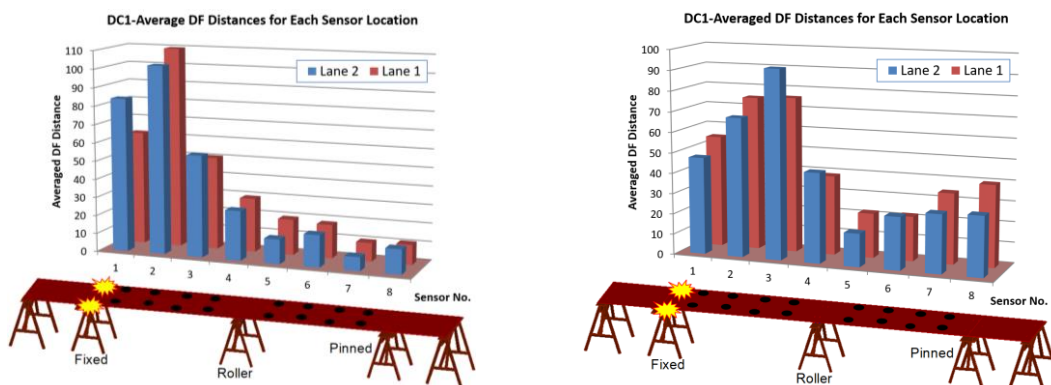


Fig. 11 Results from wired (left) and wireless clusters (right) for DC1

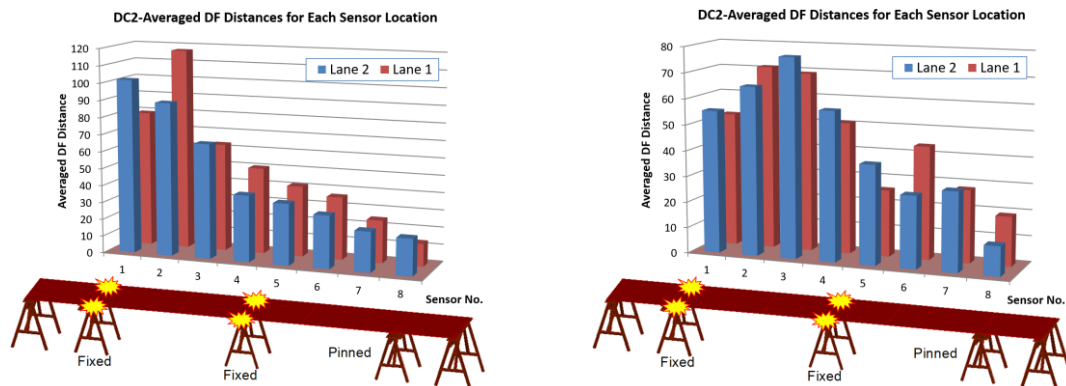


Fig. 12 Results from wired (left) and wireless clusters (right) for DC2

Plotting the data using the Averaged DF Distance method results in a much clearer visual representation of the damage magnitude at each sensor location. Fig. 11 displays the damage detection analysis results of both wired and wireless sensors for damage case 1. Nodes 1 and 9 are showing larger values than the other nodes, thus indicating damage at this region. Visual inspection of Fig. 11(left) reveals that the indication of damage decreases the farther the sensor location is from the damage location. For example, Nodes 7, 8, 15, and 16 are the farthest from the damage and have the smallest Averaged DF Distances. These results intuitively make sense, as it is expected that the dynamic properties of the structure are less affected at greater distances from the boundary condition changes. For the wireless sensor clusters, as is displayed in Fig. 11(right), it is shown that there is a higher concentration of high Averaged DF Distance values at the left span sensor locations.

When the damage detection analysis results of damage case 2 are plotted, using the Averaged DF Distances, a similar trend to DC1 is seen and shown in Fig. 12. The sensor locations nearest to the boundary condition change at the left supports continue to indicate the greatest presence of damage, as in DC1. The additional boundary change of the middle supports, however, causes an overall increase of the damage detection level in all sensors. Successful results were also realized in for the wireless sensor clusters. Comparing these results with those of DC1 for the wireless sensor clusters, it is seen that damage detection levels increased in the vicinity of the middle supports. Therefore, despite the initial display of damage detection for the left support damage appearing different, the additional boundary condition change at the middle support had the exact same impact on the data. Again, these results are consistent with the applied damage. If the boundary conditions of the structure are modified further from the baseline/healthy condition, it is expected that the entire structure should indicate this global change.

As before, higher damage levels were indicated near the left supports, at the location where the boundary conditions were modified. The addition of damage to the middle support had the impact of increasing the damage detection levels at all sensor locations. However, in both wired and wireless results for DC1, the location closest to the damage did not have the highest damage detection. In Fig. 11, showing the DC1 results, for example, the highest indication of damage is at sensor location 2 in both lanes, not at sensor location 1. In Fig. 12, showing the DC2 results, the levels of damage detection at location 1 are higher than DC1. For the wireless sensor cluster this trend is even more noticeable.

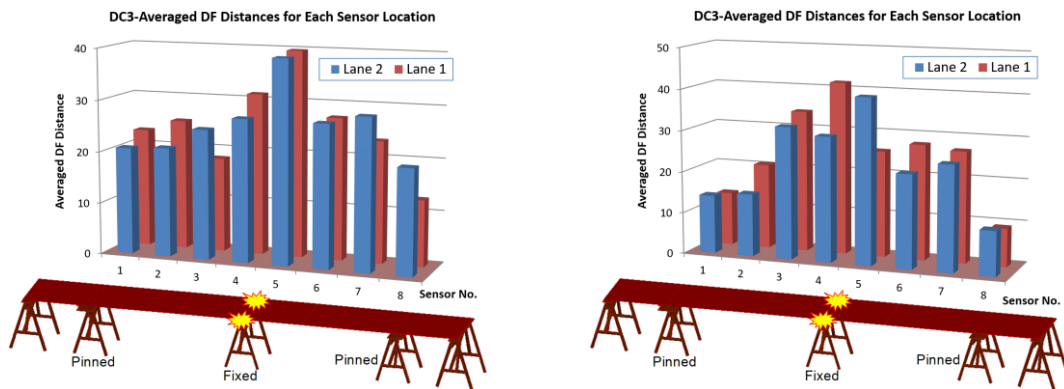


Fig. 13 Results from wired (left) and wireless clusters (right) for DC3

There are a few potential reasons for this discrepancy. The most plausible reason relates to the variation in the location of impact between the two series. Series 1 impact locations were on the decking next to the bolt connections and directly on top of the girders. The Series 2 impacts were applied to the decking, but in between the two girders. It is possible that the impulse excitation, when applied to the center of the decking, has difficulty in consistently exciting all modes of the structure at the girder sensor locations. Another possible reason for the discrepancy in results is that boundary condition changes may have not been applied in the exact same format as before. Two important points should be made, however: (1) The presence of damage is indicated throughout the structure, and (2) The largest damage indication values are located in the region of the global damage. Bearing both of these points in mind, these results can be deemed successful.

Fig. 13 shows the results of the damage case 3 analysis. The sensor locations in the region of the middle supports, where the boundary conditions were modified, are indicating a higher detection of damage. Noting the scale change of the y-axis, the Averaged DF Distances are substantially lower in magnitude in the region of damage for DC3 in comparison with those of DC1 and DC2. Although the damage scenario of DC3 represents a global condition change, fixing the pin supports at the middle location has drastically less impact on the structure in comparison to fixing the pin supports at the span ends. The reason for this is that girders over the middle supports are continuous, and due to symmetry of the structure, these middle pin supports are much more “fixed” in nature to begin with than the end of span pin supports. Therefore, changing the boundary condition to fixed at the middle supports has a less distinguishable effect on the structure dynamics.

The results from damage case 3 for the wireless sensor clusters could be considered even more explanatory than in the wired results previously seen. These results, shown in Fig. 13(right), indicate a bell type curve of damage detection values, centered on the region of damage.

Damage case 4, symmetrical to DC2, modified the boundary conditions at both the middle and right supports. The results of the damage detection analysis are shown in Fig. 14, and as expected, are very symmetrical to the results of DC2. Damage case 5, which consisted of changed boundary conditions at the right support, was a symmetrical version of DC1. The DC5 results are shown in Fig. 15. In both result plots, it is seen that detection of damage is made; however, for the wireless clusters, the indication of the region of damage, while still distinguishable, is not as clear as in the wired results. The results of DC4 and DC5 contain the same key observations as the results of

DC2 and DC1. It can be concluded that the Averaged DF Distance trends in DC4 and DC5 correspond very well with those of DC2 and DC1. These results help to qualify this damage detection method as consistent.

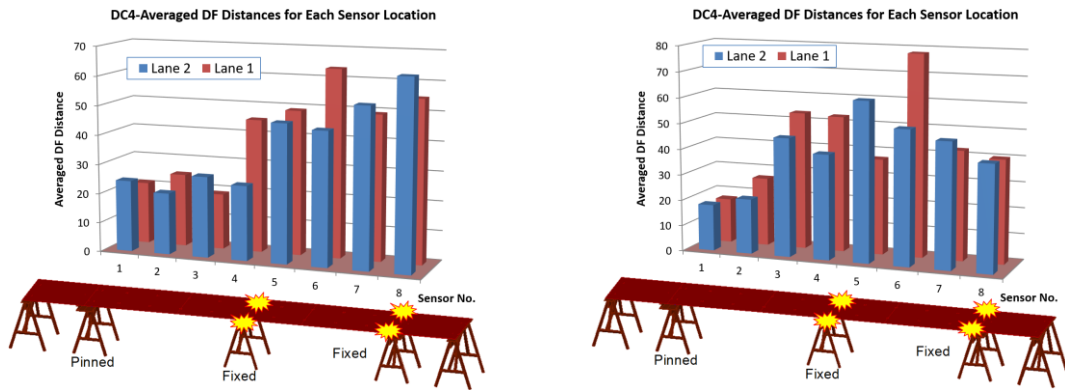


Fig. 14 Results from wired (left) and wireless clusters (right) for DC4

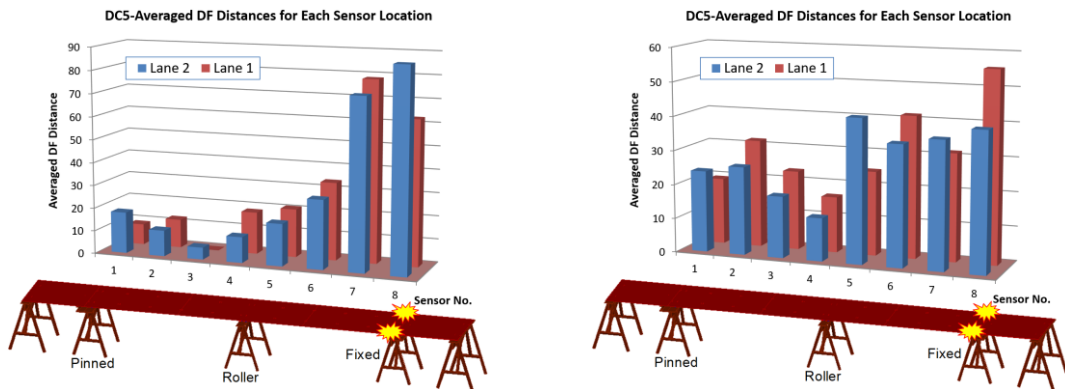


Fig. 15 Results from wired (left) and wireless clusters (right) for DC5

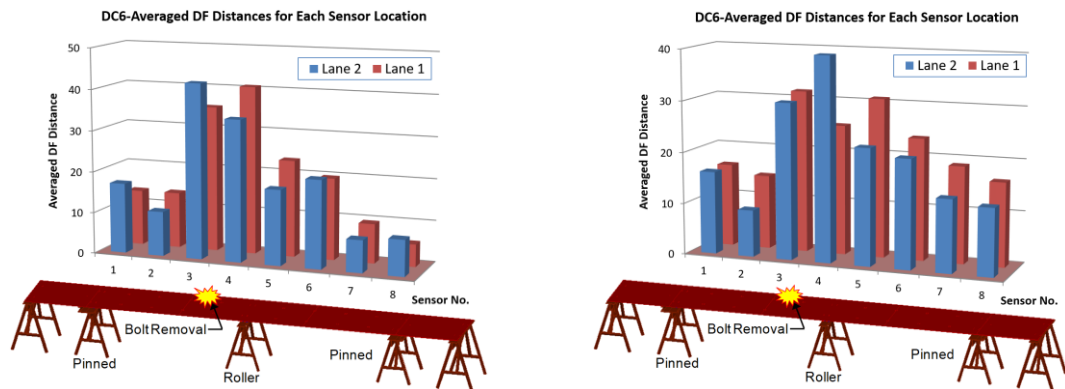


Fig. 16 Results from wired (left) and wireless clusters (right) for DC6

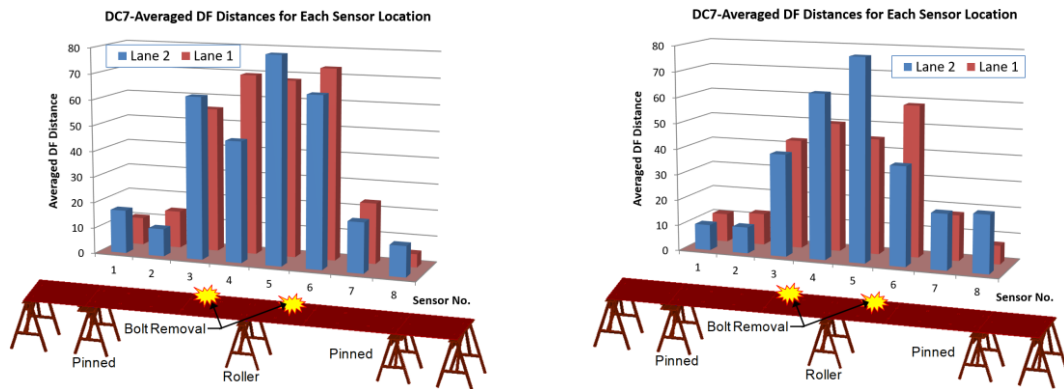


Fig. 17 Results from wired (left) and wireless clusters (right) for DC7

Moving away from the global damage scenarios, localized damage results of damage cases 6 and 7 will be presented next. The results of the damage detection analysis for damage case 6 are presented in Fig. 16. Inspection of this figure shows that the region surrounding the damage location is displaying a higher detection of damage, while the remaining sensor locations show relatively consistent, low damage levels. It is also demonstrated that the magnitude of the damage detection is much more moderate in comparison with DC1, DC2, DC4, and DC5.

Lastly, the results of damage case 7 which involved the removal of 4 more bolts from the structure at Node 6 are presented in Fig. 17. As in DC6, the results seen in DC7 demonstrate that higher damage values were again detected at the region surrounding the damage locations. This is seen from the increase in the Averaged DF Distance values in both lanes at sensor locations 5 and 6. It should be noted that the additional structural condition changes in DC7 significantly increased the magnitude of damage detection values across all sensor locations. Also, despite localized damage occurring in only one lane of both DC6 and DC7, the damage detection analysis was not able to isolate the damage to a particular lane. This is somewhat expected since the stiffness for the other lane is also reduced due to the decking system. However, seeing higher DFs for the damaged lane would have increased the value of the results significantly.

4.3 Further discussion on wireless results

Cross examination of the wireless sensor cluster results with both sets of wired results reveals a few disparities. The most obvious difference is that the wireless results consistently have lower levels of damage detection at the span ends (N1, N9, N8, N16). For example, Fig. 11 shows that for DC1, damage detection for both wired data sets (Left and Middle Column) at the left support was significantly higher than at locations nearest to the right support. However, for the wireless data (Right Column), damage detection at the left span ends was not as distinguishable. A similar trend is seen in the other damage cases where damage detection is expected to be greatest at the span ends. The possible reasoning behind these discrepancies has been investigated.

One possible reason for discrepancy relates to how the sensor clusters are defined near the boundaries. The defined sensor clusters for the span end only contain a total of 4 adjacent channels, rather than the typical 6 adjacent channels defining the other locations. Therefore, the development of the Baseline ARX models for the reference channels at the span ends only utilize 4 input sets.

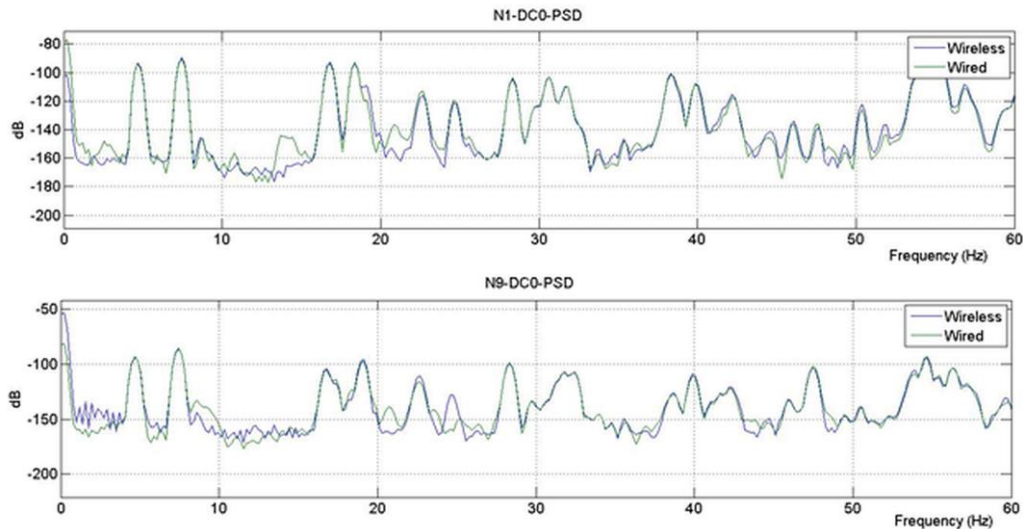


Fig. 18 Threshold Level for Wireless Series 2 Lab Study

Consequently, it is typical for the healthy condition fit ratios to be lower for the nodes representing the span ends. This trend has been observed in each of the three tests. For the wireless tests, the lower accuracy of the Baseline ARX models at the span ends may have magnified the inaccuracies of the data. Inaccuracies of the wireless data were another topic of investigation.

The verification study of the wireless sensor signals in Fig. 7 compared the time history and frequency domain content of the wireless and wired data. This investigation demonstrated that the wireless sensors had good correspondence with the wired sensors, as seen through identification of the major modes. For this reason, the wireless sensor data was deemed as adequate for application of the damage detection analysis. However, examination of the signals in the frequency domain revealed that the wireless sensors lacked identification of some of the higher frequency modes. This trend was seen across all the damage cases that were inspected. To further explore this matter, an impact from each of the end span nodes (N1, N9, N8, N16) under DC0 was examined in the frequency domain. The PSD's of N1 and N9 are shown in Fig. 18. The frequency content of the end span nodes was compared to the other nodes from the verification study to see if any causative variation could be identified. Close examination of the plots did not reveal any noticeable explanation for the end span nodes having lower damage detection levels.

5. Conclusions

The primary objective of this study was to investigate a time series based damage detection method in the context of Structural Health Monitoring (SHM), using wired and wireless sensor clusters, thereby providing more practical, less time consuming, less expensive and safer monitoring and eventually maintenance purposes. In that, ARX models were developed from different sensor clusters by using the free response of the baseline structure. The output of each

sensor in a cluster was used as an input to the ARX model, which was then used to predict the output of the reference channel of that sensor cluster. Subsequent acceleration data from that sensor cluster was input into the same ARX model, and the reference channel output was again predicted. Comparison of the predicted outputs in terms of a fit ratio was used as a Damage Feature.

The results from the wired and wireless sensor data sets showed that the ARX model damage detection methodology was effective at detecting and locating the region of damage. Both global and local damage types were able to be detected, as shown in the results. For the wireless sensor data collection, the Imote2 wireless accelerometers were introduced. A sensor roving technique was used to collect acceleration data from the entire structure using six separate sensor configurations. Both wired and wireless acceleration data were analyzed using the ARX model based damage detection method and results in the form of Averaged DF Distance plots were generated. These plots were compared for the seven experimental damage cases. The results were in very close correspondence with a few minor discrepancies. Results from the wireless data, showed a lower quality of damage localization capabilities. Possible reasons for these differences were suggested and investigation into these issues was described. Summarizing the results, it is shown that the ARX based method utilizing either wired or wireless sensors is very promising for damage detection implementation in the context of SHM.

Acknowledgments

This work was supported by National Science Foundation (NSF) Division of Civil, Mechanical, and Manufacturing Innovation (Grant No. 1463493); partially through Federal Highway Administration (FHWA) Cooperative Agreement Award DTFH61-07-H-00040. The authors would like to express their sincere gratitude for these agencies, responsible administrators, the graduate students in the Prof. Catbas' Civil Infrastructure Technologies for Resilience and Safety (CITRS) research initiative.

References

- Agha, G. and Spencer, B.F. (2011), "Getting started for advanced users and developers", Setting up the Imote2 Development Environment for TinyOS 1.x and Installing the ISHMP Services Toolsuite
- Aktan, A.E., Catbas, F.N., Grimmelsman, K.A. and Tsikos C.J. (2000), "Issues in infrastructure health monitoring for management", *J. Eng. Mech. – ASCE*, **126**(7), 711-724.
- Brownjohn, J.M.W., Tjin, S.C., Tan, G.H. and Tan, B.L. (2004), "A structural health monitoring paradigm for civil infrastructure", *Proceedings of the 1st FIG International Symposium on Engineering Surveys for Construction Works and Structural Engineering*, Nottingham, UK.
- Catbas, F.N., Brown, D.L. and Aktan, A.E. (2004), "Parameter estimation for multiple-input multiple-output modal analysis of large structures", *J. Eng. Mech. – ASCE*, **130**(8), 921-930.
- Catbas, F.N., Gul, M., Zaurin R., Gokce, H.B., Terrell, T., Dumlupinar, T. and Maier, D. (2010), "Long term bridge maintenance monitoring demonstration on a movable bridge", A Framework for Structural Health Monitoring of Movable Bridges, Florida Department of Transportation (FDOT).
- Catbas, F.N., Gul, M., Zaurin, R., Terrel, T., Dere, Y., Ansley M., Frangopol D.M., and Grimmelsman K. (2009), "Structural health monitoring for the safety of bridges: Fundamental", *Proceedings of the Application and Organizational Considerations*, ASCE Structures Congress '09, Austin, TX.

- Dessi, D. and Camerlengo, G. (2015), "Damage identification techniques via modal curvature analysis: Overview and comparison", *Mech. Syst. Signal Pr.*, **52-53**, 181-205.
- Farinholt, K.M., Miller, N., Sifuentes, W., MacDonald, J., Park, G. and Farrar, C.R. (2010), "Energy harvesting and wireless energy transmission for embedded SHM sensor nodes", *Struct. Health Monit.*, **9**(3), 269-280.
- Farrar, C.R. and Worden, K. (2007), "An introduction to structural health monitoring", *Philos. T. Roy. Soc. A*, **365**, 303-315.
- Gillich, G.R. and Praisach, Z.I. (2014), "Modal identification and damage detection in beam-like structures using the power spectrum and time-frequency analysis", *Signal Process.*, **96**, 29-44.
- Gul, M. (2009), *Investigation of damage detection methodologies for structural health monitoring*, PhD Dissertation, Department of Civil, Environmental and Construction Engineering, University of Central Florida, Orlando, FL.
- Gul, M. and Catbas, F.N. (2008), "Ambient vibration data analysis for structural identification and global condition assessment", *J. Eng. Mech.*, **134**(8), 650-662.
- Gul, M., Catbas, F.N. (2009), "A novel time series analysis methodology for damage assessment", *Proceedings of the 5th International Workshop on Advanced Smart Materials and Smart Structures Technology*, ANCRISST 2009, Boston, MA.
- Gul, M. and Catbas, F.N. (2011), "Structural health monitoring and damage assessment using a novel time series analysis methodology with sensor clustering", *J. Sound Vib.*, **330**(6), 1196-1210.
- Jang, S. and Rice, J. (2009), *Calibration Guide for Wireless Sensors*.
- Ljung, L. (1999), *System Identification: Theory for the User*. Upper Saddle River, NJ, Prentice-Hall.
- Lu, Y. and Gao, F. (2005), "A novel time-domain auto-regressive model for structural damage diagnosis", *J. Sound Vib.*, **283**, 1031-1049.
- Lynch, J.P. (2007), "An overview of wireless structural health monitoring for civil structures", *Philos. T. Roy. Soc. A*, **365**(1851), 345-372.
- Lynch, J.P., Law, K.H., Kiremidjian, A. S., Carryer, E., Farrar, C.R., Sohn, H., Allen, D.W., Nadler, B. and Wait, J.R. (2004), "Design and performance validation of a wireless sensing unit for structural monitoring applications", *Struct. Eng. Mech.*, **17**(3-4), 393-408.
- Lynch, J.P., Wang, Y., Sundararajan, A., Law, K.H. and Kiremidjian, A.S. (2004), "Wireless sensing for structural health monitoring of civil structures", *Proceedings of the International Workshop on Integrated Life-Cycle Management of Infrastructures*, Hong Kong.
- Omenzetter, P. and Brownjohn, J.M.W. (2006), "Application of time series analysis for bridge monitoring", *Smart Mater. Struct.*, **15**, 129-138.
- Pakzad, S.N. and Fenves, G.L. (2009), "Statistical analysis of vibration modes of a suspension bridge using spatially dense wireless sensor network", *J. Struct. Eng.*, **135**(7), 863-872.
- Sazonov, E., Krishnamurthy, V. and Schilling, R. (2010), "Wireless intelligent sensor and actuator network- a scalable platform for time-synchronous applications of structural health monitoring", *Struct. Health Monit.*, **9**(5), 465-476.
- Sohn, H., Czarnecki, J.A. and Farrar, C.R. (2000), "Structural health monitoring using statistical process control", *J. Struct. Eng.- ASCE*, **126**(11), 1356-1363.
- Sohn, H. and Farrar, C.R. (2001), "Damage diagnosis using time series analysis of vibration signals", *Smart Mater. Struct.*, **10**(3), 446.
- Spencer, B.F. (2011), "Getting started guide for new users", *Programming the ISHMP Toolsuite V3.0 and Collecting Data with Imote2s*.
- Spencer, B.F. (2011), "Imote2 for structural health monitoring: User's guide", *Illinois Structural Health Monitoring Project*.
- Tanner, N.A., Wait, J.R., Farrar, C.R. and Sohn, H. (2003), "Structural health monitoring using modular wireless sensors", *J. Intel. Mat. Syst. Str.*, **14**(1), 43-56.
- Zaurin, R. (2009), *Structural health monitoring with emphasis on computer vision, damage indices and statistical analysis*, Ph.D. Dissertation, Civil, Environmental and Construction Engineering Dept. Orlando, FL.

Zheng, H. and Mita A. (2009), "Localized damage detection of structures subject to multiple ambient excitations using two distance measures for autoregressive models", *Struct. Health Monit.*, **8**(3), 207-222.

JK

